Smart control based on neural networks for multicellular converters

KAMEL LAIDI[1], OUAHID BOUCHHIDA[1], MOKHTAR NIBOUCHE[2],
KHELIFA BENMANSOUR[1]

[1]University of Medea
Algeria
[2]University of the West of England
United Kingdom

e-mail: {laidi.kamel/bouchhida.ouahid/benmansour.khelifa}@univ-medea.dz

Abstract: A smart control based on neural networks for multicellular converters has been developed and implemented. The approach is based on a behavioral description of the different converter operating modes. Each operating mode represents a well-defined configuration for which an operating zone satisfying given invariance conditions, depending on the capacitors' voltages and the load current of the converter, is assigned. A control vector, whose components are the control signals to be applied to the converter switches is generated for each mode. Therefore, generating the control signals becomes a classification task of the different operating zones. For this purpose, a neural approach has been developed and implemented to control a 2-cell converter then extended to a 3-cell converter. The developed approach has been compared to super-twisting sliding mode algorithm. The obtained results demonstrate the approach effectiveness to provide an efficient and robust control of the load current and ensure the balancing of the capacitors voltages.

Key words: multicellular converters, neural networks, smart control

1. Introduction

Power electronics have well-known important technological developments. This is carried out thanks to the developments of power semiconductors and new energy conversion systems. To assume the increase of power consumption, converters have to be controlled more efficiently and increase their power. A solution to obtain both conditions is to use multilevel converters [1, 2].

Serial multicellular converters are the only solution among others that provide many degrees of freedom like the possibility to distribute the voltage constraints among serial-connected switches and improve the output waveforms [2–4]. On the other hand, the constraint of these converters is the need for a large number of capacitors, in particular for a three-phase configuration [1–3]. Despite the wide use of multicellular converters in industry as well as in research, one of the main limitations of these converters is their unregulated voltage and current [5]. To overcome this problem and ensure an efficient control, various control techniques have been developed and implemented.

The following is an overview of the well-known developed control techniques widely used in the domain. We can quote and not limit to Pulse Width Modulation (PWM), Proportional Integral (PI), Sliding Mode (SM), Hybrid and Petri Net (PN) control techniques.

In [6, 7], a high order SM controller of a mid-point multi-cellular converter is applied, while in [8] the work has focused on the state observer of a serial multicellular converter. It uses the principle of high order SM (Super Twisting) observers to force the system dynamic to converge on the so-called sliding surface [9]. A direct control based on the SM technique for a multicellular serial chopper and some solutions for direct control of the voltages across the flying capacitors, in the presence of a fast variation of the input voltage and by reaching an optimal steady-state trajectory defined by the PWM control technique is presented in [10]. In [11], a direct control strategy is proposed for a three-phase eight-level flying capacitor inverter. It is shown that the control strategy is simpler than other control algorithms proposed in the literature, like for example PWM control, and leads to less expensive hardware implementations. Moreover, its stability is proven by means of Lyapunov's theory. This approach has been compared to the conventional PWM. In [12], hybrid sliding mode control of a multicellular converter is treated. The basic idea used in this paper is to consider the interconnected systems that represent the hybrid model and generate commutation surfaces, based on a Lyapunov function to satisfy asymptotic stability. In [13], two control strategies are proposed for multicellular converters. The first one is the proportional integral control applied after feedback linearization of the studied converter model. The second one is the SM control characterized by its efficiency for nonlinear systems. In [14], two control strategies are proposed, the first is the SM control and the second is the PN control, and a comparison between them is carried out. In [15, 16], the proposed introduces the use of two PNs to carry out the control action. The first PN generates the needed voltage level to ensure the output reference current tracking, while the second PN solves the problem of capacitor voltage balancing, using switching state redundancies.

In this paper, we propose and develop a novel approach based on the Artificial Neural Networks (ANNs) for multicellular converters control. In contrary to the hybrid and Petri Nets approaches, which rely on the transition conditions between operating modes, this approach relies on the invariance conditions for each operating mode of the converter. The approach consists in classifying the different operating modes associated with their corresponding control signals by using ANNs. The rest of the paper is organized as follows: In sections 2 and 3, the behavioral modelling of serial multicellular converters and the different operating modes of a 2-cell converter are presented respectively. In section 4, a neural approach to 2-cell converter control has been developed and implemented. Then after, an extension to a 3-cell converter has taken place in section 5. Section 6, presents a comparative study between the obtained results by the neural approach and those obtained by the second order SM algorithm (Super Twisting algorithm). Finally, the conclusions drawn from this work are summarized in the conclusion section.

2. Behavioural modelling of multicellular converters

The structure of multicellular converters is based on the serialization of switching cells between which capacitor floating voltage sources are inserted. This structure can be adapted to both configurations: a chopper or an inverter, with a capacitive midpoint, half bridge or full bridge. The first advantage of this type of converters is the reduction of the voltage constraint on the switches. Floating voltage sources impose on each cell a voltage that is equal to $\frac{E}{p}$ (E is the input voltage), while the current crossing all cells is identical and equal to the load current [1]. Fig. 1 shows the diagram of the N-level arm of a p-cells converter.
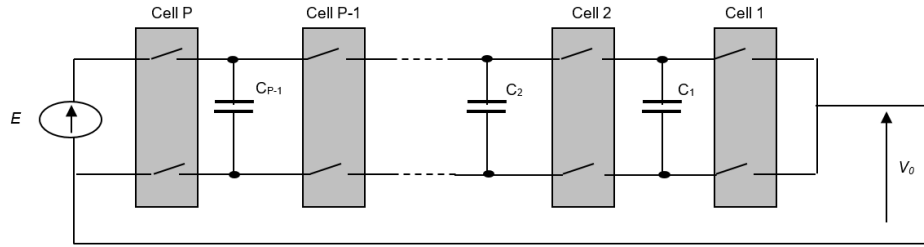
Fig. 1. *p*-cells serial converter structure

In this section, a behavioral description is adopted instead of using mathematical equations as it is usually done. It consists in classifying the different operating modes of the converter according to the floating voltages across the capacitors and the load current. Each mode represents an infinite set of the vectors $X = (V_{C1}, V_{C2}, I)$ because the current and the voltages are continuous quantities. For each mode a control vector $S = (s_1, s_2, \ldots, s_p)$, to force the converter to track their reference values given by (1), is associated.

$$X_{\text{ref}} = (V_{C1\text{ref}},\ V_{C2\text{ref}},\ I_{\text{ref}})\,. \tag{1}$$

For practical applications, the control vector has the role of keeping or bringing back the converter as much as possible in the balancing zone defined by:

$$X_{\text{ref}} \pm \Delta X_{\text{ref}} = (V_{C1\text{ref}} \pm \Delta V_{C1\text{ref}},\ V_{C2\text{ref}} \pm \Delta V_{C2\text{ref}},\ I_{\text{ref}} \pm \Delta I_{\text{ref}})\,, \tag{2}$$

where: V_{Ci} is the floating voltage across the capacitor C_i, $V_{C1\text{ref}} = \frac{iE}{P}$ is the reference voltage of the voltage V_{Ci}, I is the load current, ref is the reference load current (desired value of I), $\Delta V_{C1\text{ref}}$ is the allowable variation of V_{Ci} around $V_{Ci\text{ref}}$, ΔI_{ref} is the allowable variation value of I around I_{ref}.

When the condition $|X - X_{\text{ref}}| < \Delta X$ is satisfied, it means that the converter is operating in the balancing zone.

For reasons of simplicity, we give the abbreviated notations to the following electrical quantities:

$$I_{\text{ref}}^- = I_{\text{ref}} - \Delta I_{\text{ref}}\,, \tag{3}$$

$$I_{\text{ref}}^+ = I_{\text{ref}} + \Delta I_{\text{ref}}\,, \tag{4}$$

$$V_{Ci\text{ref}}^{+} = V_{Ci\text{ref}} + \Delta V_{Ci\text{ref}}, \tag{5}$$

$$V_{Ci\text{ref}}^{-} = V_{Ci\text{ref}} - \Delta V_{Ci\text{ref}}. \tag{6}$$

where: $V_{Ci\text{ref}}^{+}$ and $V_{Ci\text{ref}}^{-}$ are, respectively, the maximal and the minimal allowed reference voltage across the capacitor $C_i I_{\text{ref}}^{+}$ and I_{ref}^{-} are, respectively, the maximal and the minimal allowed value of the current flowing through the circuit.

Our development for synthesizing a neural control approach targets two classes of converters: the first one is a 2-cell converter and the second one is a 3-cell converter.

Before starting, it is worth remembering that each of the cell switches works in a complementary way, i.e. when the upper switch is 'ON' the lower switch is 'OFF' and vice versa. The control signal s_k is equal to '1' when the upper switch of the cell is conducting and '0' when the lower complementary switch of the cell is conducting.

3. Configuration of 2-cell converter

According to the principle of multicellular converters, four possible configurations or modes (q_0, q_1, q_2, q_3) are possible for 2-cell converters, which are given by [16, 17]:

$(s_2, s_1) = \{(0, 0), (0, 1)(1, 0)(1, 1)\}$, as it is illustrated in Fig. 2(a), Fig. 2(b), Fig. 2(c) and Fig. 2(d).

Mode $q_0 = (s_2, s_1) = (0, 0)$

In this mode, no voltage source is applied to the load; we are in a free-wheel phase. The floating capacitor voltage does not change, while the load current decreases exponentially. The system remains in this mode as long as the current is not less than I_{ref}^{-} and the floating voltage remains balanced, or if the current is greater than I_{max} (Fig. 2(a)).
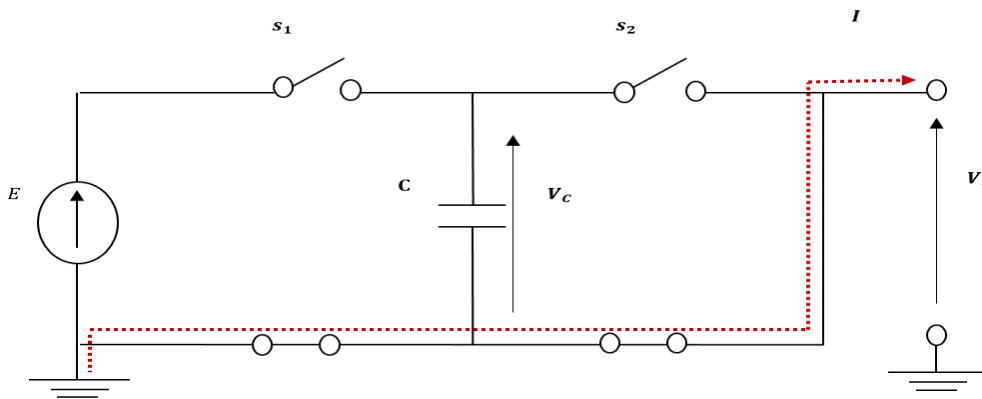
Fig. 2(a). 2-cell converter in mode q_0

Mode $q_1 = (s_2, s_1) = (0, 1)$

The energy is provided by the floating source. The capacitor is discharged and its energy is returned to the load. The system remains in this mode as long as the capacitor voltage does not

decrease below V_{Cref}^+ and the current is between its minimal value I_{min} and its maximal value I_{max} or if the converter is operating in the balancing zone (Fig. 2(b)).
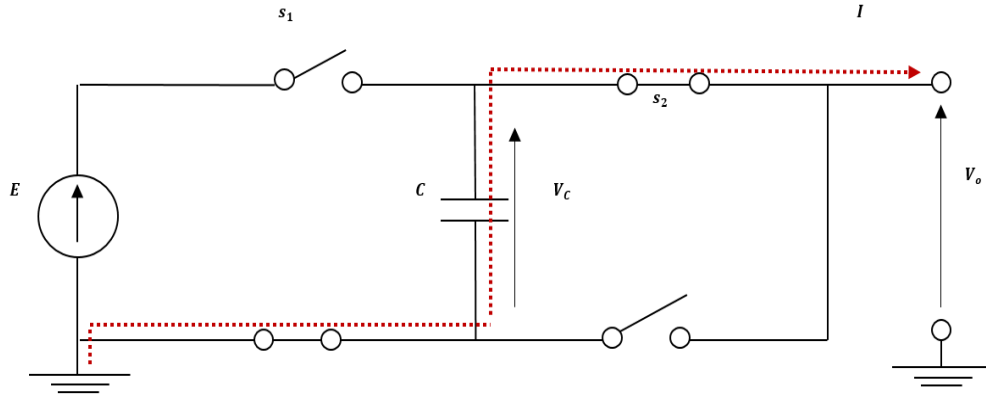
Fig. 2(b). 2-cell converter in mode q_1

Mode $q_2 = (s_2, s_1) = (1, 0)$

In this mode, the capacitance takes on importance, and the energy is supplied by the source E. The system remains in this mode as long as the capacitor voltage does not exceed V_{Cref}^- and the current is between I_{min} and I_{max} or if the converter is working in the balancing zone (Fig. 2(c)).
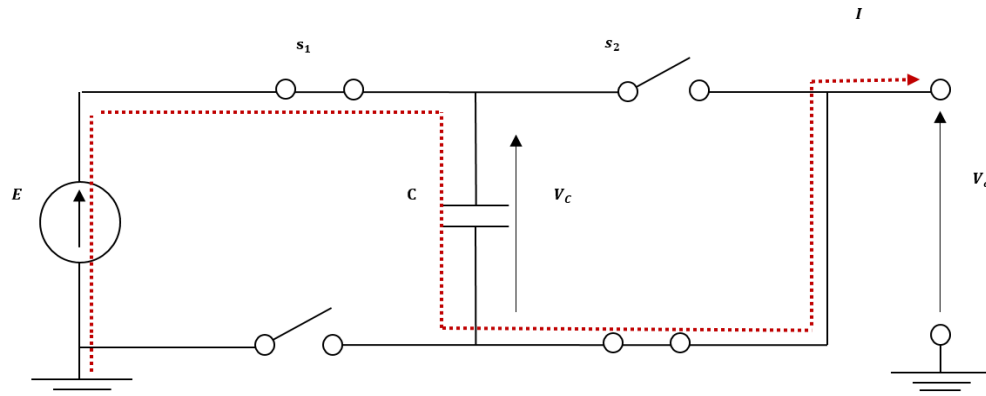
Fig. 2(c). 2-cell converter in the mode q_2

Mode $q_3 = (s_2, s_1) = (1, 1)$

In this mode, the energy is supplied by the source E. The load current increases and the voltage across the capacitor remains constant. The system remains in this mode as long as the current does not exceed I_{ref}^+ and the capacitor voltage is between V_{Cref}^- and V_{Cref}^+ or if the current is less than I_{min} (Fig. 2(d)).

Noting that the floating source participates in the evolution of the system dynamics only in the modes q_1 and q_2, i.e. $(s_2, s_1) = \{(0, 1), (1, 0)\}$. Thus, if these modes continue for the same
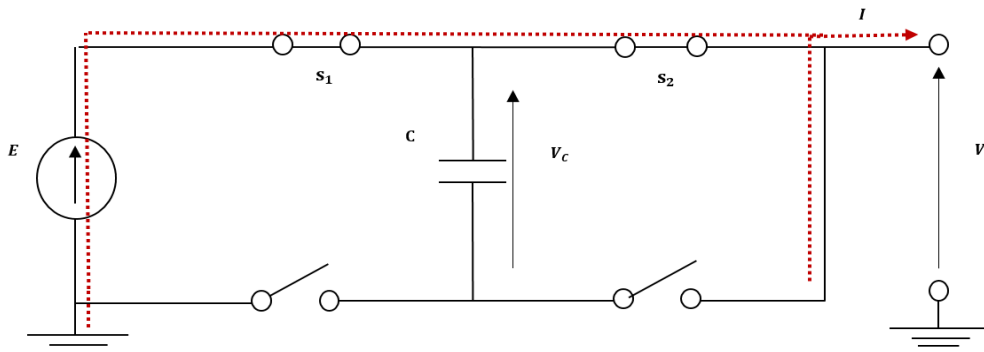
Fig. 2(d). 2-cell converter in the mode q_3

time with a constant charging current, then the average power transmitted by the floating source over a switching period is zero. We note also that these two modes allow obtaining the additional level $\dfrac{E}{2}$ at the output voltage V_0.

Fig. 3 illustrates graphically the invariance conditions, where each mode condition forms a continuous space delimited by a correspondent voltage and current intervals, and for which the balancing zone belongs to all modes [1].
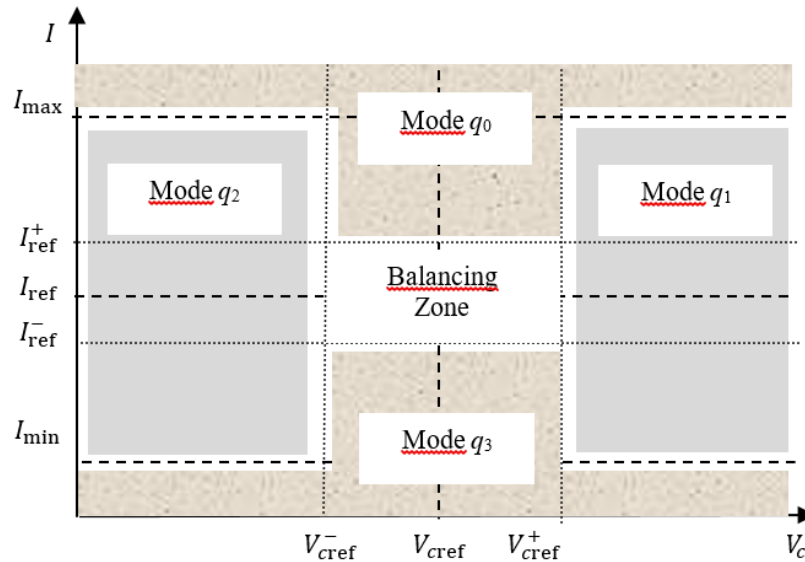
Fig. 3. Operating mode zones in 2-cell converter

The analytical invariance conditions for each mode, i.e. the condition $X(q_i)$ for which the converter remains in the mode q_i are expressed by Equations (7), (8), (9) and (10) [1].

We mentioned that $|V_C - V_{Cref}| < \Delta V$ means $V_{Cref}^- < V_C < V_{Cref}^+$ and $(|I - I_{ref}| < \Delta I$ means $I_{ref}^- < I < I_{ref}^+$. Therefore, the invariance conditions are given as follows: (7) for the mode q_0, (8) for the mode q_1 (9) for the mode q_2 and (10) for the mode q_3, as it is illustrated respectively in Fig. 2(a), Fig. 2(b), Fig. 2(c) and Fig. 2(d).

$$X(q_0) = \left\{ X \in R^2 : \left[(|V_C - V_{Cref}| < \Delta V) \wedge (I_{ref}^- < I < I_{max}) \right] \vee (I > I_{max}) \right\}, \tag{7}$$

$$X(q_1) = \left\{ \begin{array}{c} X \in R^2 : \left[V_C > V_{Cref}^+ \right) \wedge (I_{min} < I < I_{max}) \right] \\ \vee \left[(|V_C - V_{Cref}| < \Delta V) \wedge (|I - I_{ref}| < \Delta I) \right] \end{array} \right\}, \tag{8}$$

$$X(q_2) = \left\{ \begin{array}{c} X \in R^2 : \left[V_C < V_{Cref}^- \right) \wedge (I_{min} < I < I_{max}) \right] \\ \vee \left[(|V_C - V_{Cref}| < \Delta V) \wedge (|I - I_{ref}| < \Delta I) \right] \end{array} \right\}, \tag{9}$$

$$X(q_3) = \left\{ X \in R^2 : \left[(|V_C - V_{Cref}| < \Delta V) \wedge (I_{min} < I < I_{ref}^+) \right] \vee (I < I_{min}) \right\}. \tag{10}$$

4. Neural control approach

Fig. 4 is the global scheme of the neural controller for 2-cell converter constituted of:
– An input layer (2 inputs) for V_C and I.
– Two hidden layers, with 6 neurones for each one.
– An output layer (two outputs) for s_2 and s_1.
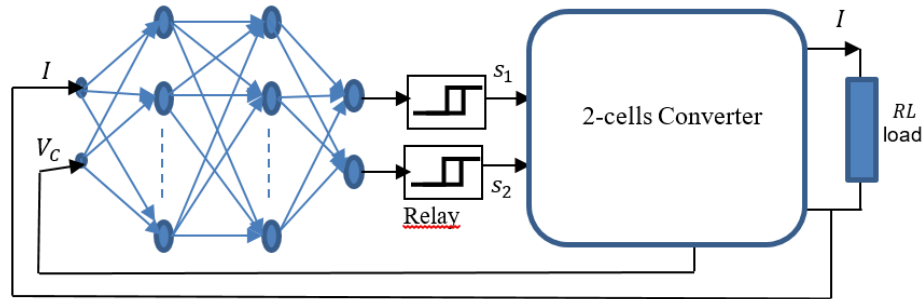
Fig. 4. Global scheme of 2-cell neural converter controller

A sigmoid activation function has been used in the hidden layer and a linear activation function has been used in the output layer. Since that the computed outputs (the net outputs) are never exactly equal to '0' or '1', two relays have been inserted to force the output to zero '0' if it is inferior to a lower threshold (set to 0.2) or to one '1' if it is superior to a higher threshold (set to 0.8) as it is shown in Fig. 4.

4.1. Learning phase

The performance of an ANN depends heavily on what it has learned. Hence, in order to generate vectors (V_C, I) that present all possible cases that may be encountered during the converter work; we have done a uniform sampling of the operating mode zones (more than

900 vectors have been generated). The components of the vectors (V_C, I) are normalized with respect to V_{Cref} and I_{ref}, respectively and associated with their corresponding outputs (s_2, s_1) to form the training patterns. The vectors normalization allows one to use the neural controller for different values of V_{Cref} and I_{ref}. The size of training patterns is a compromise between the ANN complexity and the desired precision. It is worth noting that for the cases where I and V_C are not bounded ($I > I_{max}$ in the mode q_0 and $V_C > V_{Cref}^+$ in the mode q_1), we have limited the surface sampling to $2I_{max}$ for I and to $2V_{Cref}$ for V_C, which is considered largely sufficient (see Fig. 5).
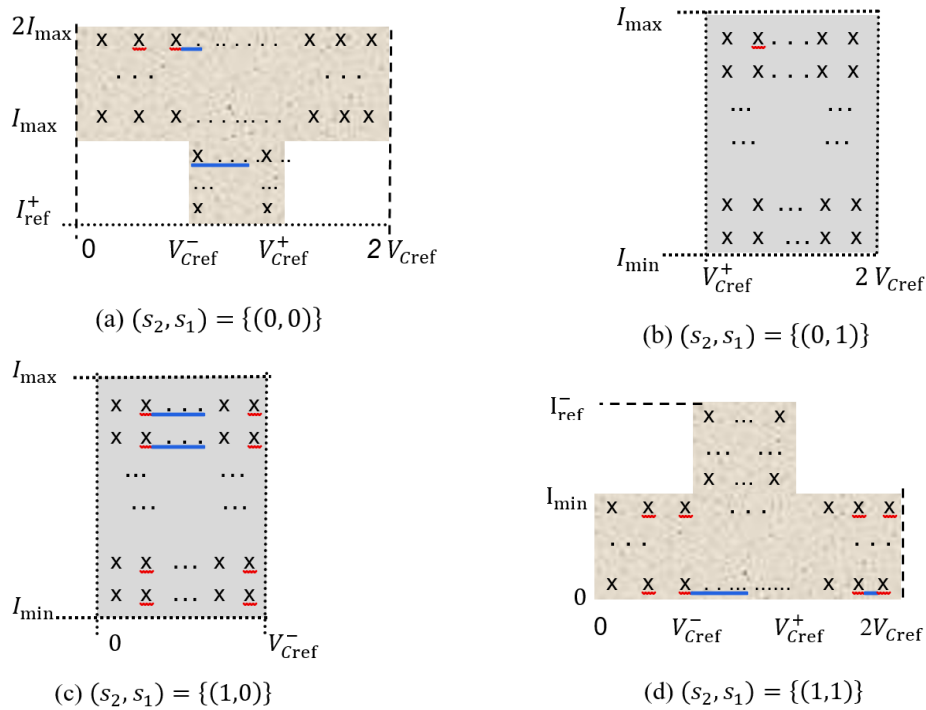
Fig. 5. Sample vectors $\{(V_C, I)\}$ for neural net training

It should also be pointed out, that the balancing zone is not considered by the training patterns since it belongs to all the modes. Hence, if the converter slides to this zone, (s_2, s_1) remains unchanged until its exit.

A supervised learning using the famous Back-Propagation Algorithm (BPA), with the following parameters:

$$E = 1200 \text{ V}, \quad \Delta V = 2\% V_{Cref}, \quad I_{ref} = 80 \text{ A}, \quad \Delta I = 2\% I_{ref},$$

has been performed and a convergence precision of 10^{-12} has been reached. The difficulty met in the learning phase lies in the input patterns choice, especially in the zone borders which prevent the algorithm convergence. Once the convergence is reached, the network is ready to be used by the application.

4.2. Application phase

MATLAB allows converting the neural network to a Simulink block that will be inserted into the global control diagram. The electrical diagram of the neural controller associated with a 2-cell converter is illustrated in the appendix (see Fig. A1).

The application of a 2-cell chopper connected to RL load, with the following parameters:

$$C = 40\ \mu\text{F}, \quad R = 10\ \Omega, \quad L = 0.5\ \text{mH},$$

has given excellent results, as they are shown in Fig. 6 and Fig. 7, either for the capacitors voltages balancing or for the load current control.

(a) Evolution of the capacitor voltage V_C (b) Zoom of the capacitor voltage V_C

Fig. 6

(a) Evolution of the load current I (b) Zoom of the load current
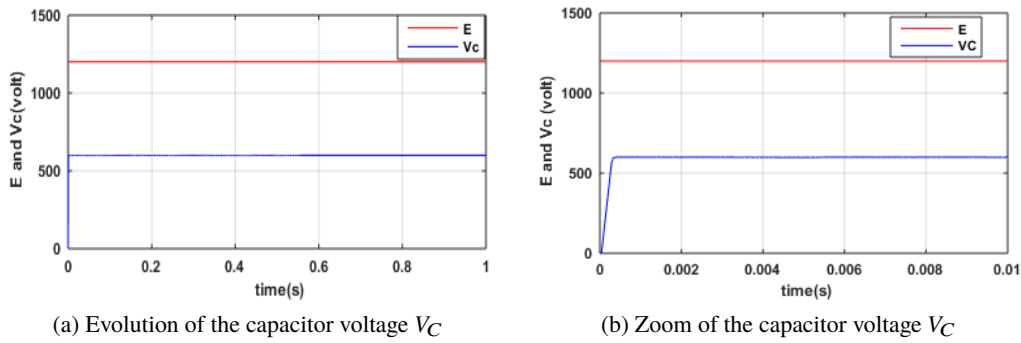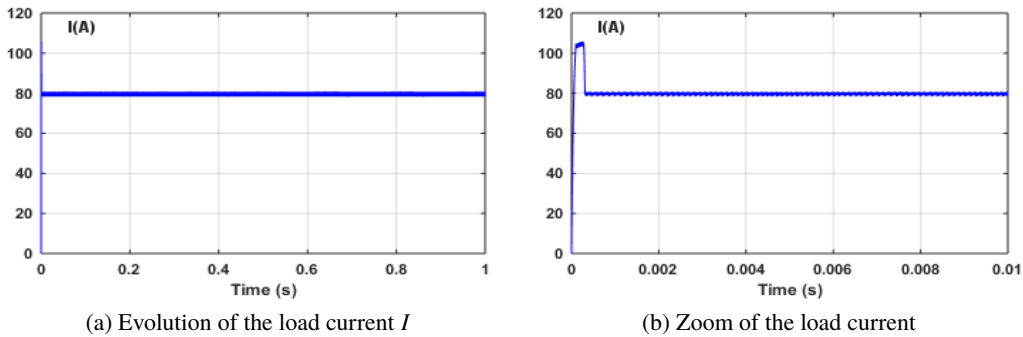
Fig. 7

5. Extension to 3-cell converter

We consider a 3-cell converter, which connects in series three elementary cells. As the switching orders of the cells are independent, one obtains ($2^3 = 8$) possible configurations, which are illustrated by the following figures (Fig. 8(a) to Fig. 8(h)). At the output voltage V_0, one obtains four possible levels $\left(0, \dfrac{E}{3}, \dfrac{2E}{3}, E\right)$.

(a) $T_0 (s_3 = 0; s_2 = 0; s_1 = 0)$ (b) $T_1 (s_3 = 0; s_2 = 0; s_1 = 1)$

(c) $T_2 (s_3 = 0; s_2 = 1; s_1 = 0)$ (d) $T_3 (s_3 = 0; s_2 = 1; s_1 = 1)$

(e) $T_4 (s_3 = 1; s_2 = 0; s_1 = 0)$ (f) $T_5 (s_3 = 1; s_2 = 0; s_1 = 1)$

(g) $T_6 (s_3 = 1; s_2 = 1; s_1 = 0)$ (h) $T_7 (s_3 = 1; s_2 = 1; s_1 = 1)$
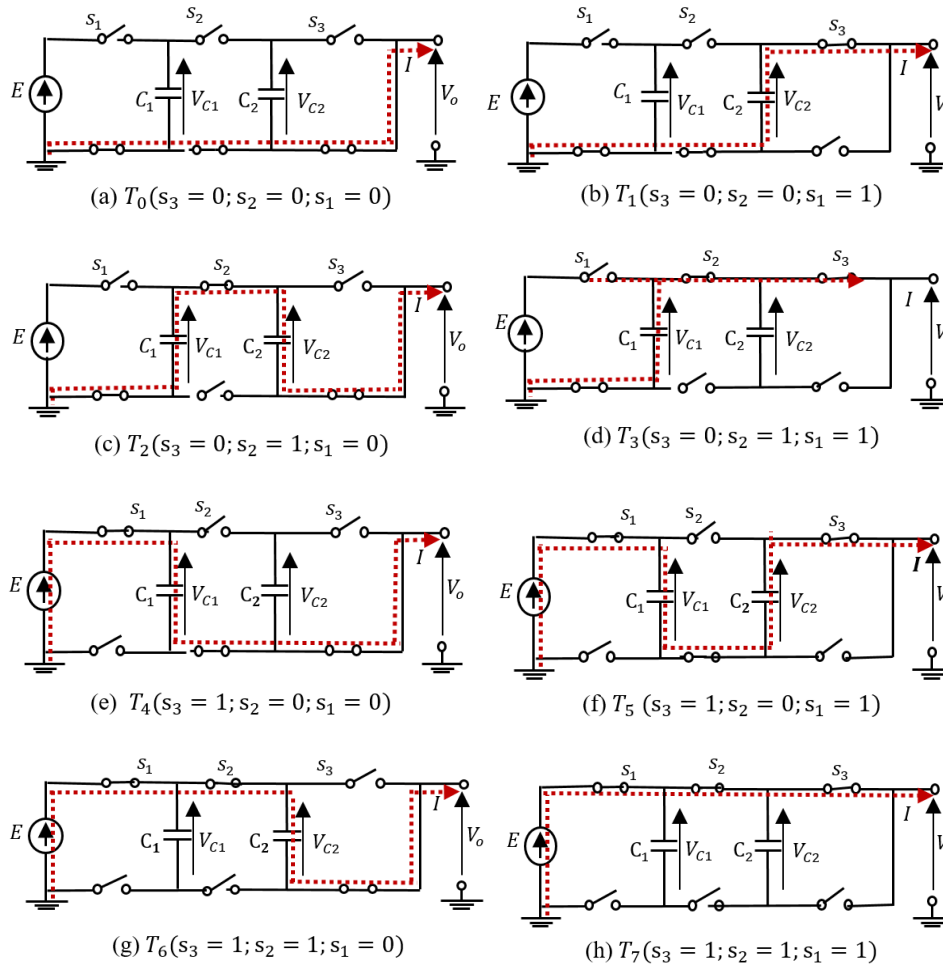
Fig. 8. 3-cell converter modes

Now, the question that arises is how to elaborate the invariance conditions with 3 variables and for each mode? Our idea is as follows: since the current flowing through all cells is the same, we consider a 3-cell converter as a juxtaposition of 2-cell converters, where the middle cell is used by both 2-cell converters and the voltage V_C is replaced by V_{C1} for the first converter and by V_{C2} for the second converter. Therefore, each 3-cell converter mode can be obtained by combining 2-cell converter modes. The invariance conditions for a 3-cell converter is a logical '**and**' between two invariance conditions of 2-cell converters.

For an analytical writing, we adopt the following notation:

$X_1 (q_i)$ is the invariance condition in the mode q_i for the first 2-cell converter,

$X_2 (q_i)$ is the invariance condition in the mode q_i for the second 2-cell converter,

$X (T_i)$ is the invariance condition in the mode T_i for the 3-cell converter.

Therefore, we can explain the invariance conditions $\{X(T_i)\}$ by the following set of equations (11)–(18).

$$X(T_0) = X_1(q_0) \text{ and } X_2(q_0), \tag{11}$$

$$X(T_1) = X_1(q_0) \text{ and } X_2(q_1), \tag{12}$$

$$X(T_2) = X_1(q_1) \text{ and } X_2(q_2), \tag{13}$$

$$X(T_3) = X_1(q_1) \text{ and } X_2(q_3), \tag{14}$$

$$X(T_4) = X_1(q_2) \text{ and } X_2(q_0), \tag{15}$$

$$X(T_5) = X_1(q_2) \text{ and } X_2(q_1), \tag{16}$$

$$X(T_6) = X_1(q_3) \text{ and } X_2(q_2), \tag{17}$$

$$X(T_7) = X_1(q_3) \text{ and } X_2(q_3). \tag{18}$$

For example, Fig. 9 shows a 3-cell converter in the mode $T_5(s_3 = 1; \ s_2 = 0; \ s_1 = 0)$ as a combination of the mode $q_2(s_3 = 1; \ s_2 = 0)$ and the mode $q_1(s_2 = 0; \ s_1 = 1)$.
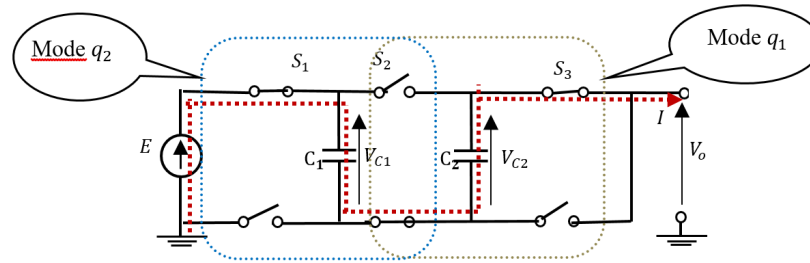
Fig. 9. T_5 as combination of q_2 and q_1

The invariance condition for this mode given by (16) can be obtained by a logical 'and' between the invariance condition of the mode q_2 for the first 2-cell converter and the invariance condition of the mode q_1 for the second 2-cell converter.

$X_1(q_2)$ and $X_2(q_1)$ are deduced directly from (8), (9) and given by (19a), (19b) as follows:

$$X_1(q_2) = \left\{ \begin{array}{l} X \in R^2: \ \left[\left(V_{C2} < V_{C2\text{ref}}^-\right) \wedge (I_{\min} < I < I_{\max})\right] \\ \vee \left[(|V_{C2} - V_{C2\text{ref}}| < \Delta V) \wedge (|I - I_{\text{ref}}| < \Delta I)\right] \end{array} \right\}, \tag{19a}$$

$$X_2(q_1) = \left\{ \begin{array}{l} X \in R^2: \ \left[\left(V_{C1} > V_{C1\text{ref}}^+\right) \wedge (I_{\min} < I < I_{\max})\right] \\ \vee \left[(|V_{C1} - V_{C1\text{ref}}| < \Delta V) \wedge (|I - I_{\text{ref}}| < \Delta I)\right] \end{array} \right\}. \tag{19b}$$

Based on these conditions, more than 27 000 input vectors whose components are (V_{C1}, V_{C2}, I) associated with their corresponding output vectors whose components are $(s_1, s_2$ and $s_3)$ have been generated by a program separately. A neural network having the following structure:

– an input layer of 3 inputs for V_{C1}, V_{C2} and I,
– two hidden layers of 10 neurones each,
– an output layer of three neurones for s_1, s_2 and s_3,

has been developed. Furthermore, the same convergence precision for the 2-cell converter has been obtained using the following parameters:

$$E = 1200 \text{ V}, \quad V = 2\% V_{Cref}, \quad I_{ref} = 80 \text{ A}, \quad \Delta I = 2\% I_{ref}.$$

Now, the neural controller is ready to be inserted into the control scheme. The electrical scheme of the neural controller associated with the 3-cell converter is illustrated in the appendix (see Fig. A2 in the appendix).

For the following converter parameters: $C_1 = C_2 = 40 \text{ μF}$ and for different RL loads (resistive loads and inductive loads), the obtained results for the capacitors voltage and for the load current evolution are shown in Fig. 10 and Fig. 11.

5.1. Evolution of the capacitor voltages V_{C1} and V_{C2}

In this section, we present the evolution of the voltages V_{C1} and V_{C2} for four different loads. This is done by applying four different combinations (resistance–inductance), the values of which are given as follows:

$$R = 10 \text{ Ω}, \ L = 0.1 \text{ mH}, \ R = 10 \text{ Ω}, \ L = 1 \text{ mH}, \ R = 1 \text{ Ω}, \ L = 10 \text{ mH}, \ R = 1 \text{ Ω}, \ L = 100 \text{ mH}.$$

In Fig. 10, the evolution of V_{C1} and V_{C2} is illustrated for the first 10 000 μs of the inverter operating, which is the period that represents the critical phase; where the big change at the floating capacitor voltages occurs. Therefore, the voltages V_{C1} and V_{C2} converge respectively to

(a) $R = 10 \text{ Ω}, L = 0.1 \text{ mH}$

(b) $R = 10 \text{ Ω}, L = 1 \text{ mH}$

(c) $R = 1 \text{ Ω}, L = 10 \text{ mH}$

(d) $R = 1 \text{ Ω}, L = 100 \text{ mH}$
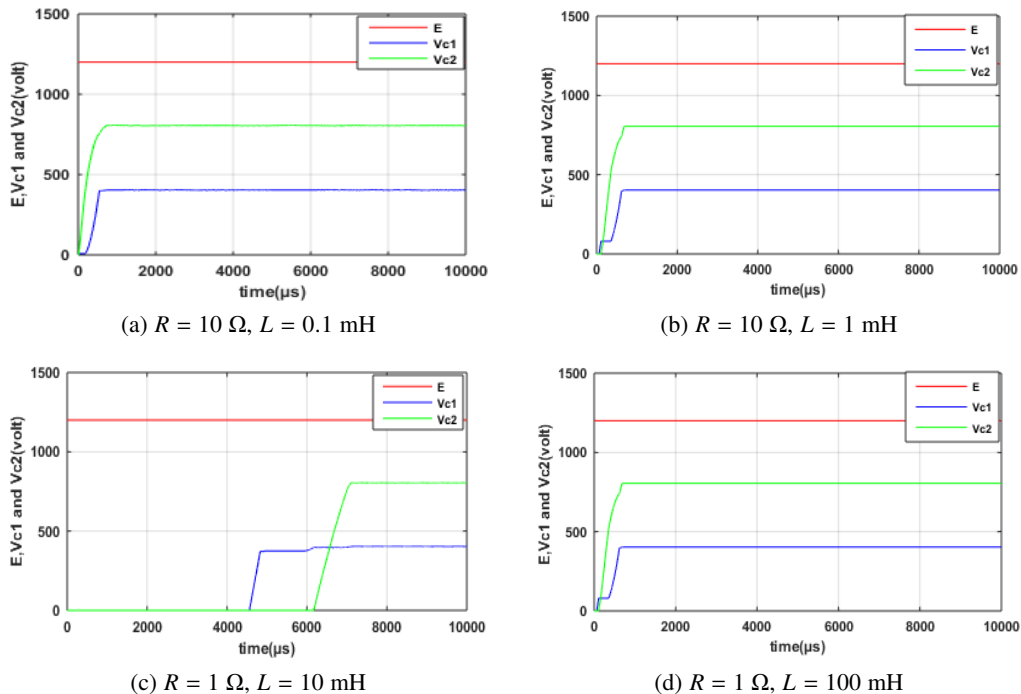
Fig. 10. Evolution of the voltages V_{C1} and V_{C2}

their desired values $\dfrac{E}{3}$ and $\dfrac{2E}{3}$ and consequently, the capacitors voltage balancing is realized. What is remarkable and concluded from the above figures is that the convergence time (settlement time) increases each time the value of the inductance increases, i.e. the load becomes more and more inductive.

5.2. Evolution of the load current *I*

In this section, we present the evolution of the load current for four different loads as we have done for the floating voltages in the previous section: $R = 10\ \Omega$, $L = 0.1$ mH, $R = 10\ \Omega$, $L = 1$ mH, $R = 1\ \Omega$, $L = 10$ mH, $R = 1\ \Omega$, $L = 100$ mH.

It is very clear that the load current converges to its reference $I_{\text{ref}} = 80$ A after a transition time, which varies depending on the load nature. Each time, the load becomes more inductive, the transition time increases and the trajectory of the evolution of the load current becomes smoother (the current ripples decrease) (Fig. 11).

(a) $R = 10\ \Omega$, $L = 0.1$ mH   (b) $R = 10\ \Omega$, $L = 1$ mH

(c) $R = 1\ \Omega$, $L = 10$ mH   (d) $R = 1\ \Omega$, $L = 100$ mH
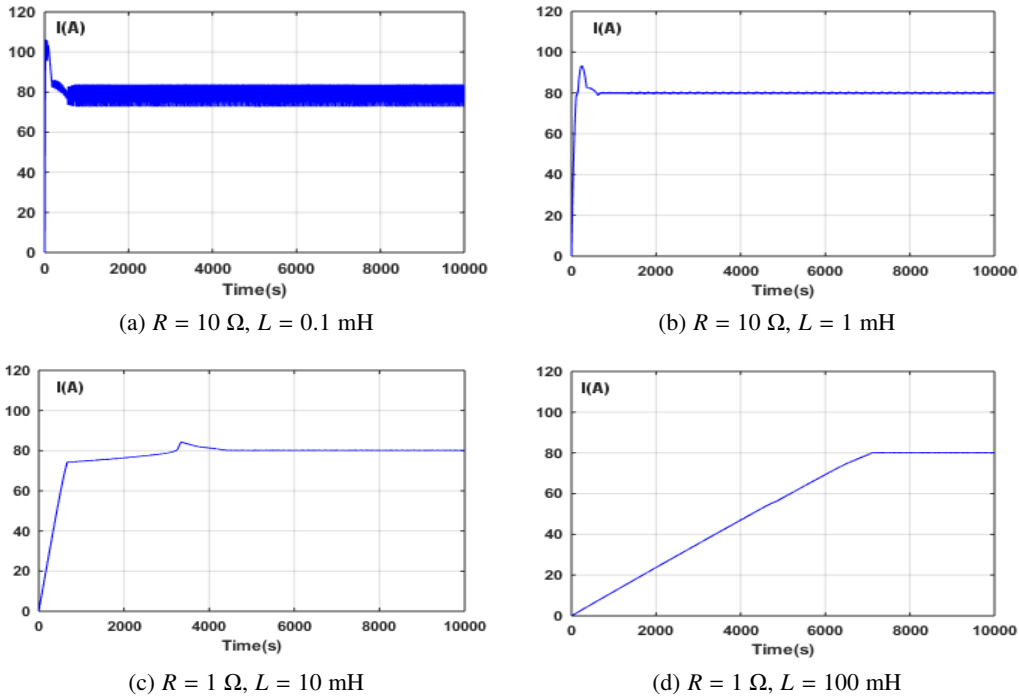
Fig. 11. Evolution of the load current *I*

5.3. Control sequences

Fig. 12(a) shows the transition between modes during the time range [0 µs, 1000 µs] for the 3-cell converter connected to *RL* load ($R = 1\ \Omega$, $L = 1$ mH). In this period, a large number of transitions between modes occurs with an irregular manner, on the contrary to the permanent

regime in which the transitions between modes are regular. The neural controller generates automatically the control sequence according to its inputs (I, V_{C1} and V_{C2}).

For a better visibility of the transitions diagram, a zoom of two-time ranges [0 μs, 200 μs] and [600 μs, 700 μs] has been provided (see Fig. 12(c) and Fig. 12(b)).
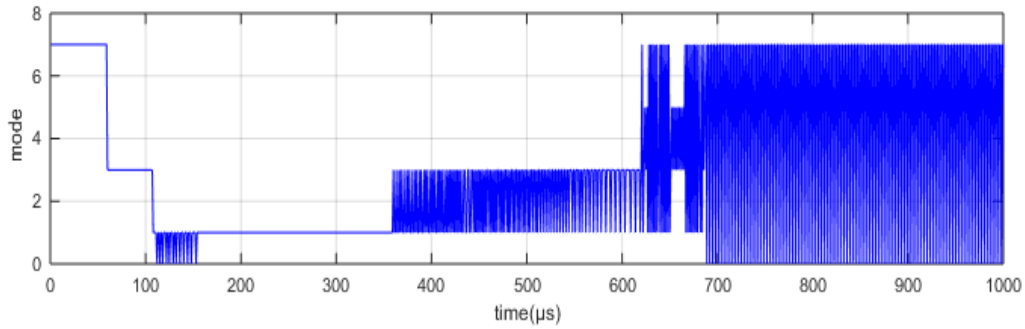
(a) Transitions between modes for 3-cell converter ($R = 1$ Ω, $L = 1$ mH)
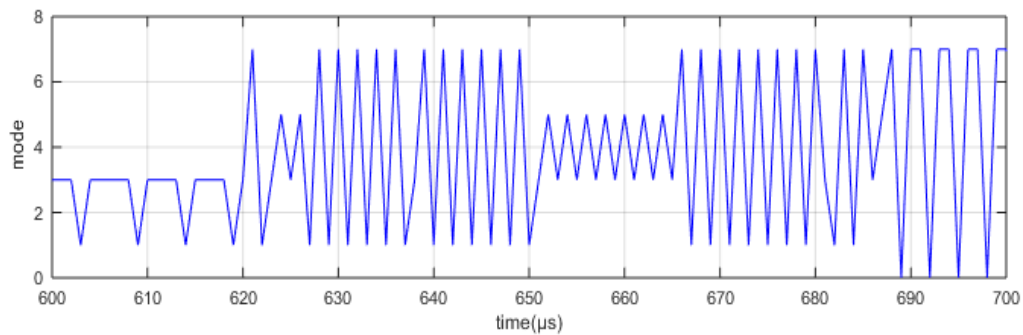
(b) Zoom of the transitions in the time range [600 μs, 700 μs]
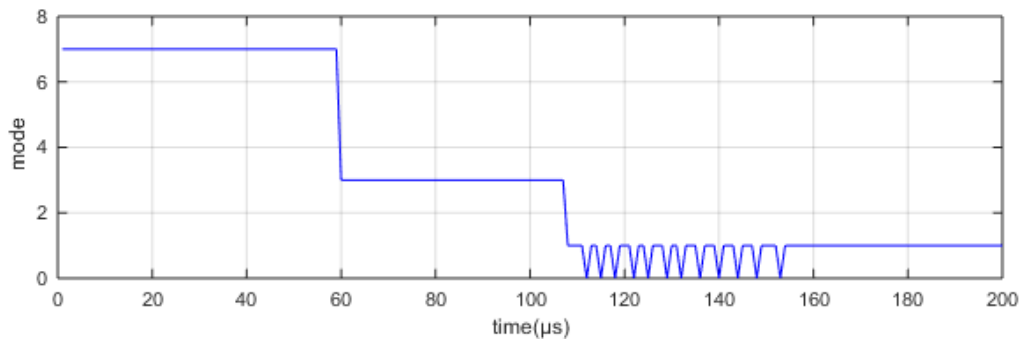
(c) Zoom of the transitions in the time range [0 μs, 200 μs]

Fig. 12

In order to show the control sequence and to confirm its correspondence with the operating modes of the converter, the evolution of s_3, s_2 and s_1 during [0 μs, 200 μs] has been illustrated in Fig. 12(d).
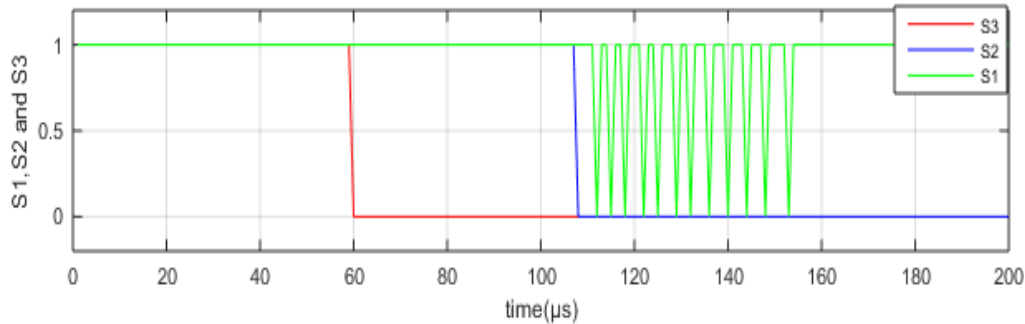
(d) Evolution of s_1, s_2 and s_3 during [0 μs, 200 μs]

Fig. 12

6. Comparison with the sliding mode approach

To better show the performance of our developed approach (neural approach), a comparative study with the Sliding Mode approach (the famous second order SM algorithm called Super Twisting) is presented in this section. The study focuses on the evolution of the floating capacitors voltages V_{C1} and V_{C2} and the load current, for different load values seen in section 5. The left column (column a) presents the results related to the neural approach and the right column (column b) presents the results related to the SM approach, as it is illustrated in Fig. 13 and Fig. 14.

Fig. 13 shows that the balancing of the floating voltages is ensured by both approaches, nevertheless it is a little faster and regular in the case of the SM approach. Fig. 14 shows that the evolution of the load current obtained by the neural approach is very close and presents similar performances to that obtained by the SM approach; which justifies the efficiency and the correctness of the neural approach.

7. Conclusion

A smart control based on artificial neural networks for multicellular converters has been developed and implemented. It has been shown that this approach constitutes a very efficient tool for the control of multicellular converters, in terms of either accuracy or settlement time, especially when doing good learning for the neural network. In addition to the very satisfactory results obtained in our application, the controller can be used by other applications having other reference values for the capacitors voltages and the load current; this requires only a simple normalization of the capacitors voltages and the load current before being entered into the
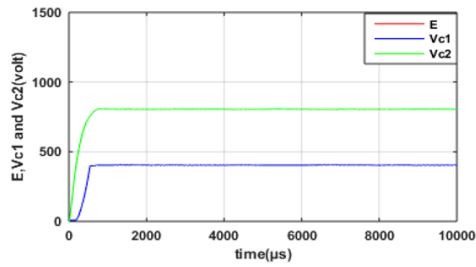
(a) 1
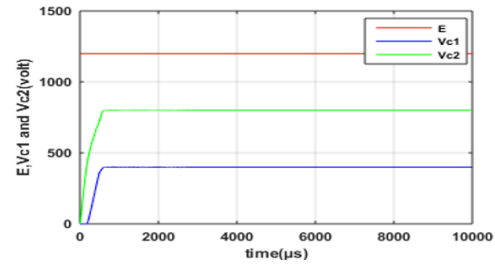
(b) 1
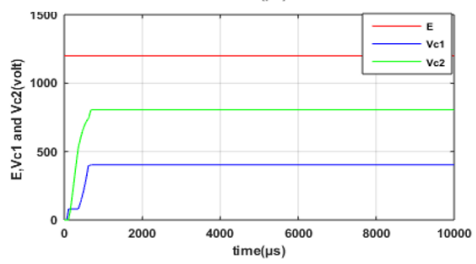
(a) 2
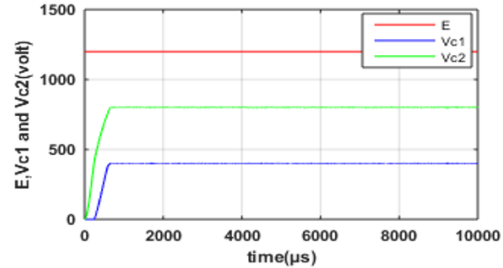
(b) 2
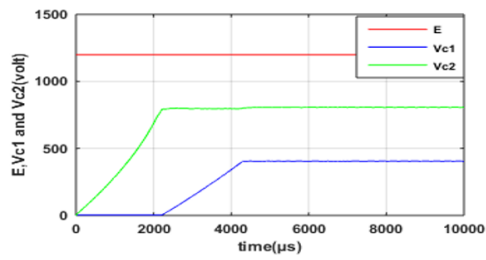
(a) 3
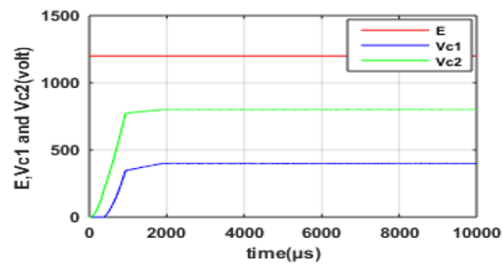
(b) 3
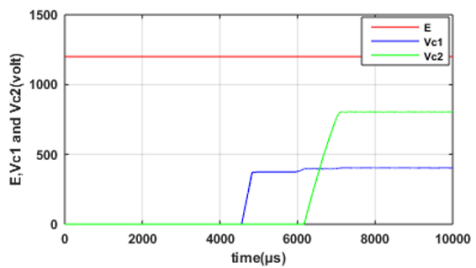
(a) 4
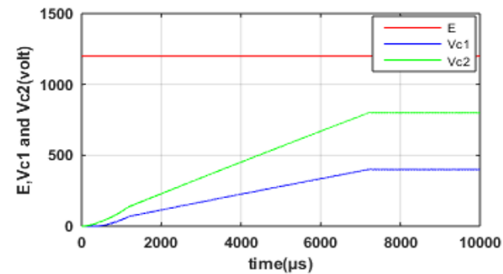
(b) 4

Fig. 13. Evolution of V_{C1} and V_{C2} in the neural and in the SM approaches, column (a) – the neural approach; column (b) – the SM approach. (a) 1 and (b) 1: $R = 1\ \Omega$, $L = 0.1$ mH; (a) 2 and (b) 2: $R = 1\ \Omega$, $L = 1$ mH; (a) 3 and (b) 3: $R = 1\ \Omega$, $L = 10$ mH; (a) 4 and (b) 4: $R = 1\ \Omega$, $L = 100$ mH
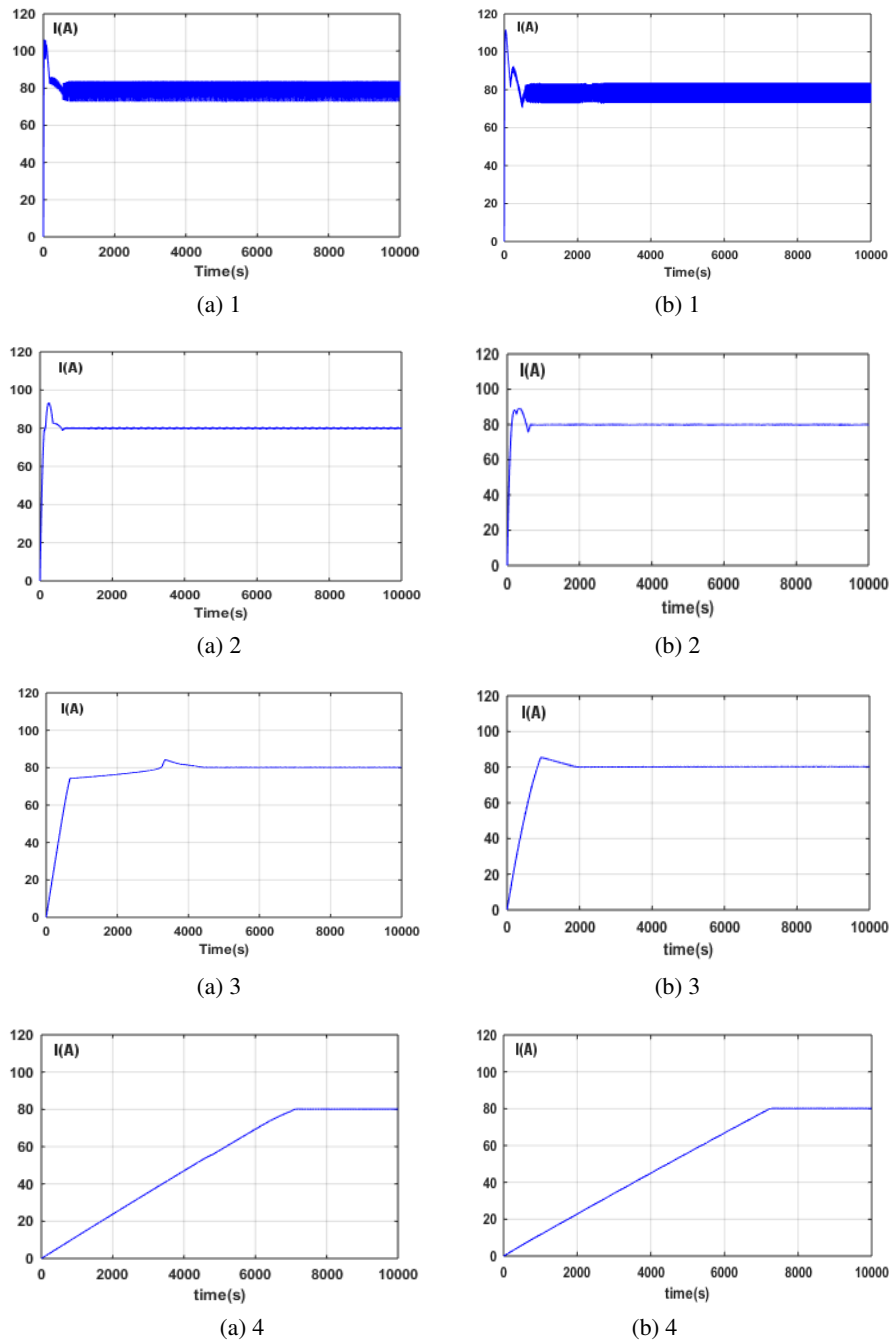
Fig. 14. Evolution of the load current I in the neural approach and in the SM approach, column (a) – the neural approach; column (b) – the SM approach. (a) 1 and (b) 1: $R = 1\ \Omega$, $L = 0.1$ mH; (a) 2 and (b) 2: $R = 1\ \Omega$, $L = 1$ mH; (a) 3 and (b) 3: $R = 1\ \Omega$, $L = 10$ mH; (a) 4 and (b) 4: $R = 1\ \Omega$, $L = 100$ mH

neural controller. Since this approach is based on a behavioural description of the converter, no mathematical equations development is required. Furthermore, the neural approach works independently of the operating point of the converter, hence the control law is insensitive to the changes in the operating point and the converter dynamics.

The difficulty was in generating the learning pattern vectors for a 3-cell converter that encompasses all cases which may be encountered during the converter operating. To overcome this problem, a novel idea has been developed and implemented.

Appendix

The electrical schemes below illustrate the Simulink neural control modules connected to the multi-cell converter (chopper in our case). For both cases, 2-cell and 3-cell converters, it is worth noting that the converter structure is developed manually using Simulink/SimPower, while the neural net modules (neural controllers) are generated automatically by the Matlab program once the learning phase is achieved. Afterwards, each module is inserted into the corresponding global scheme to ensure the converter control. The component named 'convert' in the scheme is to convert the input to the data type and scaling of the output. We also point out that these electrical schemes appear a little blurry since they have been inserted directly from the Simulink environment.
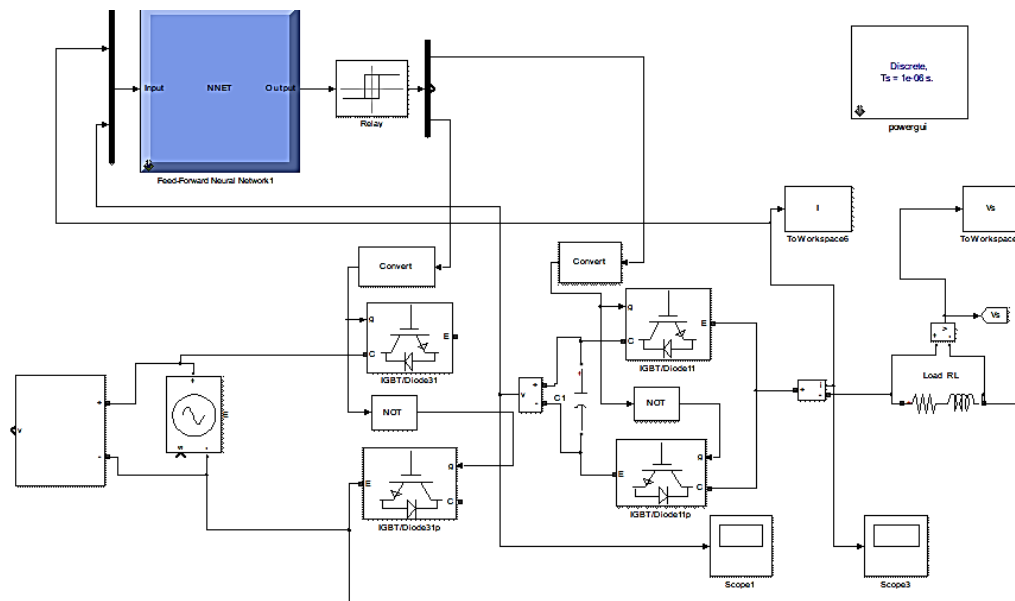
Fig. A1. The electrical scheme of 2-cell converter connected to its neural controller
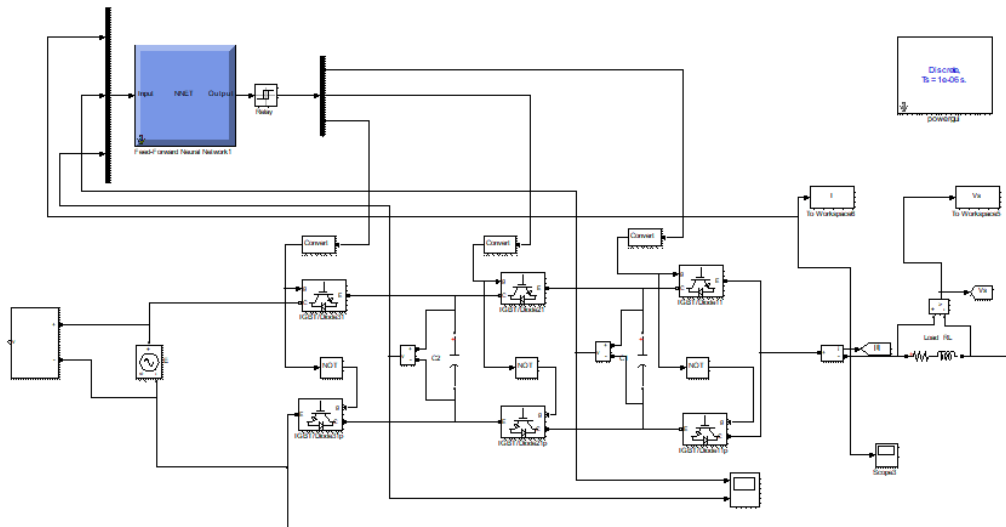
Fig. A2. The electrical scheme of 3-cell converter connected to its neural controller

References

[1] Benmansour K., *Réalisation d'un banc d'essai pour la Commande et l'Observation des Convertisseurs Multicellulaires séries*, Approche Hybride, PhD Thesis, Université de Cergy Pontoise, France (2009).

[2] Colak I., Kabalci E., Bayindira R., *Review of multilevel voltage source inverter topologies and control schemes*, Energy Conversion and Management Journal, vol. 52, iss. 2, pp. 1114–1128 (2011).

[3] Laidi K., Benmansour K., Ferdjouni A., Bouchhida O., *Real-time implementation of an interconnected observer design for p-cells chopper*, Archives of Electrical Engineering, vol. 59, no. 2, pp. 5–20 (2010).

[4] Meynard T., Foch H., *Multilevel choppers for high voltage applications*, European Power Electronics and Drives Journal, vol. 2, no. 1, pp. 45–50 (1992).

[5] Meynard T., Foch H., *Electronic device for electrical energy conversion between a voltage source and a current source by means of controllable switching cells*, European Patent 92/91 6336.8 (1992).

[6] Laidi K., Benmansour K., *High Order Sliding Mode Controller of Mid-point Multi-cellular Converter*, 2nd International Symposium on Friendly Energy and Applications, Newcastle Upon Tyne, pp. 493–498 (2012).

[7] Pinon D., *Commande des Convertisseurs Multicellulaires par Mode de Glissement*, PhD Thesis, INPT, Toulouse (2000).

[8] Skender M.R., Tlemçani A., *A New Algorithme Observer of Higher Order Sliding Mode Applied to Serial Multicell Converter*, Revue Roumaine des Sciences Techniques – Série Électrotechnique et Énergétique, vol. 61, no. 2, pp. 126–130 (2016).

[9] Zhang H., Dong H., Zhang B., Tong Wu, Changwen Chen, *Research on beam supply control strategy based on sliding mode control*, Archives of Electrical Engineering, vol. 69, no 2, pp. 349–364 (2020).

[10] Amet L., Ghanes M., Barbot J.P., *Direct control based on sliding mode techniques for multicells serial chopper*, American Control Conference, San Francisco, CA, USA (2011).

[11] Laamiri S., Ghanes M., Amet L., Santomenna.G, *Direct Control Strategy for a Three Phase Eight-Level Flying-Capacitor Inverter*, IFAC Journal of Systems and Control, vol. 50, iss. 1, pp. 15786–15791 (2017).

[12] Benzineb O., Taibi F., Benbouzid M.E., Boucherit M.S., Tadjine M., *Multicell Converters Hybrid Sliding Mode Control*, IFAC World Congress 2014, Cape Town, South Africa, pp. 11659–11666 (2014).

[13] Bensaid S., Bensaad K., Benrejeb M., *On Two Control Strategies for Multicellular Converters*, International Journal of Control, Energy and Electrical Engineering (CEEE), vol. 1, pp. 37–42 (2014).

[14] Djondine P., Barbot J.P., Ghanes M., *Comparison of sliding mode and petri nets control for multicellular chopper*, International Journal of Nonlinear Science, vol. 25, no. 2, pp. 67–75 (2018).

[15] Salinas S., Ghanes M., Barbot J.P., Escalante F., Amghar B., *Modeling and Control Design Based on Petri Nets for Serial Multicellular Choppers*, IEEE Transactions on Control Systems Technology, vol. 23, no. 1 (2015).

[16] Derugo P., Żychlewicz M., *Reproduction of the control plane as a method of selection of settings for an adaptive fuzzy controller with Petri layer*, Archives of Electrical Engineering, vol. 69, no. 3, pp. 609–624 (2020).

[17] Manon P., Valentin C.R., Gilles G., *Optimal Control of Hybrid Dynamical Systems: Application in Process Engineering*, Control Engineering Practice, pp. 133–149 (2002).

[18] Teel A.R., Bonivento C., Isidori A., Marconi L., Rossi C., *Robust hybrid control systems: an overview of some recent results*, Advances in Control Theory and Applications, Springer, vol. 353, pp. 279–302 (2007).